Light impurity transport in JET ILW L-mode plasmas

N. Bonanomi[1,2], P. Mantica[2], C. Giroud[3], C. Angioni[4],
P. Manas[4], S. Menmuir[3]and JET contributors*

EUROfusion Consortium, JET, Culham Science Centre, Abingdon, OX14 3DB, UK

1) University of Milano-Bicocca, Milano, Italy

2) CNR- Institute of Plasma Physics "P. Caldirola", Milano, Italy

3) Culham Centre for Fusion Energy, Abingdon, OX14 3DB, UK

4) Max Planck Institute for Plasma Physics, Boltzmannstr. 2, 85748 Garching, Germany

* See the author list of See the author list of "X. Litaudon et al., 2017 Nucl. Fusion **57**, 102001"

Abstract

A series of experimental observations of light impurity profiles was carried out in JET (Joint European Torus) ITER-like wall (ILW) L-mode plasmas in order to investigate their transport mechanisms. These discharges feature the presence of $^3He, Be, C, N, Ne$, whose profiles measured by active Charge Exchange diagnostics are compared with quasi-linear and non-linear gyro-kinetic simulations. The peaking of ^3He density follows the electron density peaking, Be and Ne are also peaked, while the density profiles of C and N are flat in the mid plasma region. Gyro-kinetic simulations predict peaked density profiles for all the light impurities studied and at all the radial positions considered, and fail predicting the flat or hollow profiles observed for C and N at mid radius in our cases.

1 Introduction

Puffing light impurities at the plasma edge is one of the ways to reduce the heat loss deposition on the divertor of ITER (International Thermonuclear Experimental Reactor) and perhaps of a future reactor [1, 2]. ^4He will be produced in the plasma central core region by the $D-T$ fusion reactions. Furthermore, ITER will have a first wall made of beryllium. While decreasing the power at the edge by increasing the radiative power could help to reduce the damages on the machine walls and on the divertor, an accumulation of impurities in the core could lead to a dilution of the main ion species that will participate to the reactions. Understanding how these light impurities are transported in the plasma is then fundamental in order to predict the best scenarios for future machines and achieve optimal conditions for fusion.

In the last years, both experimental and theoretical investigations on light impurity transport have been made in various machines [3-10]. In many conditions, turbulent transport dominates the transport of light impurities in a tokamak plasma core. The main mechanisms that drive the turbulent particle transport have been identified [11-16] and their relative importance for different impurities and plasma conditions has been investigated. Despite all the efforts, some differences are still present between the predicted peaking of light impurities and the experimental values. In JET [3, 5, 8] and ASDEX Upgrade [3] H-mode plasmas, differences between the experimental density peaking of $^3He, C$, B and Ni and the predicted peaking by gyro-kinetic and neoclassical theory have been found, while in DIII-D [17] H-mode plasmas, differences between density peaking of F and quasi-linear and neoclassical predictions have been observed, indicating that something may be missing for a complete understanding of the particle transport of light impurities. With respect to previous

JET studies made in C-wall H-modes, this study was performed in JET ILW L-modes, increasing the number of light impurities studied, by measuring in the same discharges the profiles of $^3He, Be, C, N$ and Ne with different heating schemes. Whilst C and Be as intrinsic impurities and ^3He as ICRH minority species were present in all discharges, N and Ne were puffed in some of them. Furthermore, mainly plasmas with low rotation have been studied, in order to minimize the impurity transport terms linked to rotation and test the model performance in this limit. The experimental results are shown and studied through neoclassical and gyro-kinetic simulations, which indicate that, in the studied plasmas, turbulent transport is the dominant transport mechanism, while neoclassical transport plays a minor role.

The paper is organized as follows. In sections 2 and 3 the experimental and numerical set-up and methods are reviewed. Section 4 discusses the study of the light impurity density profiles. A discussion on the results and the conclusions are presented in section 5.

2 Experimental set-up

The discharges studied in this paper were made in two different experimental sessions (n. 86739-86759 from one session and n. 90666-90672 from the other) in the JET tokamak (major radius $R_0 = 2.96\,m$, minor radius $a = 1\,m$) with ILW. The two sessions have very similar experimental settings and plasma parameters. All plasmas are D plasmas with vacuum toroidal magnetic field $B_T \approx 3.3\,T$, plasma current $I_p \approx 2\,MA$ and safety factor at the flux surface that encloses the 95% of the poloidal flux $q_{95} \approx 5$. The heating power consists of 2.5-7 MW of ICRH (Ion Cyclotron Resonance Heating) using a ^3He minority concentration $n_{^3He}/n_e \approx 6-9\%$, which ensures a dominant ion heating [18], and of 1.7-3 MW of NBI (Neutral Beam Injection) , mainly to provide charge exchange measurements of T_i, plasma rotation Ω_t and impurity density profiles. In all the studied discharges the RF power was deposited on-axis ($R \approx 3.0\,m$). The discharges analyzed were all L-modes, apart from two discharges (n. 86758 and n. 86759) where the NBI heating was increased to 13 MW, in order to study the effect of the presence of higher rotation and plasma beta , changing the plasma condition from L-mode to H-mode.

The measurement of the electron temperature T_e is provided by the ECE (Electron Cyclotron Emission) diagnostic with an error on the measurements of about 5%, while the ion temperature T_i and plasma rotation ω_T are measured by the CX (Charge-Exchange) diagnostic with an error of about 5-10%, depending on the radial position, for the ion temperature and of about 10% for the plasma rotation. The error on T_e/T_i is about 9–12%. The electron density n_e is measured by high-resolution Thomson scattering (HRTS) with an uncertainty of about 15%. Local values of $R/L_{Ti} = -R_0\nabla T_i/T_i, R/L_{Te} = -R_0\nabla T_e/T_e$ and $R/L_n = -R_0\nabla n_e/n_e$ were obtained by local linear fits of $ln(T_i), ln(T_e)$ and $ln(n_e)$ radial profiles averaged over a time interval $\Delta t \approx 1\,s$. The fits are done using $r = (R-R_{in})/2$, R and R_{in} being the outer and inner boundaries of the flux surface on the magnetic axis plane, and averaging other multiple fits using a variable number of data points around the chosen radius (3-9 points). We drop the suffix 0 when indicating these quantities for convenience. The uncertainties on these parameters are then estimated by repeating the same procedure with different space intervals and evaluating the deviation in the set of values so obtained. Errors are typically 10-15% for $R/L_{Te/i}$ and 15-20% for R/L_n. The radial profile of the safety factor q as well as the equilibrium plasma geometry are reconstructed by the EFIT equilibrium code with the MSE (Motional Stark Effect) or the Faraday rotation constraints. Typical errors on the safety factor are about 20%. Radial profiles of T_e, T_i, n_e, q and Ω_t of discharges n. 86740 (L-mode with 3 MW of ICRH + 3 MW of NBI, $n_{^3He}/n_e \sim 6\%, n_{Be}/n_e \sim 1\%, n_C/n_e \sim 0.1\%$), n. 86749 (L-mode with 4 MW of ICRH + 3 MW of NBI, $n_{^3He}/n_e \sim 6\%, n_{Be}/n_e \sim 1\%, n_C/n_e \sim 0.1\%, n_N/n_e \sim 1.2\%$), n. 86758 (H-mode with 2.5 MW of ICRH + 13 MW of NBI, $n_{^3He}/n_e \sim 8\%, n_{Be}/n_e \sim 1\%, n_C/n_e \sim 0.1\%, n_N/n_e \sim 1\%$) and n. 90670 (L-mode with 6 MW of ICRH + 1.7 MW of NBI, $n_{^3He}/n_e \sim 9\%, n_{Be}/n_e \sim 1\%, n_C/n_e \sim 0.1\%, n_{Ne}/n_e \sim 0.1\%$) are shown in *figure 1*. The parameters of these shots have been used as input in the simulations for the study of the impurity transport. The ICRH power deposition of discharge n. 90670, obtained with the SELFO code [19, 20], is shown figure 1.

The data analysis is carried out at $\rho_{tor} = 0.33, 0.5, 0.7\rho_{tor} = \sqrt{(\Phi/\pi B_T)/(\Phi/\pi B_T)_{max}}$, where Φ is the toroidal magnetic flux.

2.1 Charge exchange impurity measurements

All the density profiles of the light impurities studied in this work have been measured using the charge-exchange diagnostic. C ($n_C/n_e \sim 0.1\%$) and Be ($n_{Be}/n_e \sim 1\%$) were present in all the discharges as intrinsic impurities and ^3He ($n_{He}/n_e \sim 6-10\%$) was puffed into all discharges as ICRH minority species. N ($n_N/n_e \sim 1\%$) was puffed in discharges n. 86749-86759 to study its effect on thermal transport while Ne ($n_{Ne}/n_e \sim 0.1\%$) was puffed in shots n. 90666 - 90672 to optimize the charge-exchange measurements.

The JET Core CXRS diagnostic consists of two periscopes that define toroidal views aligned on the heating neutral beams of octant 8. A neutral beam injector consists of two sets of four positive ion neutral injectors (PINIs) divided into the so-called tangential and normal bank. Due to the arrangement of the heating beams, the toroidal views aligned on PINI 6 (normal) and 7 (tangential) also intersect PINI 1 (tangential). As a result, for each viewing direction, a set of three volumes defines the average spatial position of the measured quantities as well as the radial resolution.

Two rows of sightlines per periscope provide a profile measurement for the low field side edge to the plasma core. The spectral analysis of the plasma light collected by the two periscopes can be performed with five spectrometers and profiles are obtained with 12-15 spatial points with 10ms time resolution. In this paper He/Be-CX spectra, C/Ne-CX spectra ad N-CX spectra was obtained each by one of these rows. The knowledge of the alignment of periscope sightlines with the PINIs is important for the determination for T_i, V_ϕ and, in particular for this paper, the impurity density n_{imp}. Geometrical factors enter the determination of n_{imp}. The exact distance of the probe volumes from the axis of the PINI has a direct impact on the impurity density determined in the line of sight and thereby on the inferred impurity density profile. Any inaccuracy in the periscope alignment corresponds to a systematic error in the value of the impurity density but also to a systematic error in the impurity density profile. An alignment technique has been developed consisting of three steps: the alignment in laboratory , the in-vessel alignment and the use of the so-called He doping and PINI switching calibration shots, described in more detail in [21], which reduce the uncertainty due to alignment to a few %.

As for the analysis for the CX spectra, during the JET C-wall years, the CXRS analysis mostly relied on multi-gaussian fit without the use of the beam modulation technique [22]. Since JET ILW, due to the reduction of the intrinsic C concentration and also to the increase in the intensity of nuisance lines, the CXRS analysis is now relying on the use of beam modulation. This consists in subtracting passive frames, where only the passive emission is collected, from active frames, where both charge-exchange emission and passive emission are collected. Provided that the active and passive frames where collected in equivalent plasmas, we should obtain a single Gaussian shape to fit the active signal of the PINI considered. The difficulty in this technique is the identification of active and passive frames that can be considered equivalent. Experimentally, it was found that the selection of passive frames with the lowest edge nuisance lines (Be-II line in the CVI-CX or He/Be-CX spectra and N-II line in N-CX spectra) and corresponding active frames with the intensity of the nuisance line within 20% of the reference passive frame results in a nice Gaussian. This technique has been used for the data presented in this paper.

The CX Helium measurements are known to be affected by the plume effect [23, 24]. Since a precise quantitative treatment of the helium plume effect is not yet available for the JET charge exchange diagnostics, this effect is not taken into account in this work and only the uncorrected values of $R/L_{n,^3He}$ are reported. Such correction is expected not to vary much with radius, therefore possibly affecting the absolute values of the ^3He density but not much its profile peaking, which is what is addressed by our study.

3 Numerical simulation set-up

The density n of each species in the plasma satisfies the continuity equation

$$\frac{\partial n}{\partial t} = -\nabla \cdot \Gamma_n + S_n \tag{3.1}$$

where Γ_n is the particle flux and S_n is the source of the particles. The particle flux of an arbitrary species in the plasma can be written as

$$\Gamma_n = n\left(-D_n \frac{\partial ln(n)}{\partial r} + V_n\right) \tag{3.2}$$

where D_n is the diffusion coefficient of the diagonal diffusive term and V_n is the convection velocity of the off-diagonal convective term. The particle flux can be written as a sum of the neoclassical particle flux [25] and the turbulent particle flux [26] $\Gamma_n = \Gamma_n^{neo} + \Gamma_n^{turb}$.

A further decomposition of the turbulent particle transport is [26, 27]

$$\frac{R\Gamma_n^{turb}}{n} = D_n \frac{R}{L_n} + RV_n = D_n \frac{R}{L_n} + D_T \frac{R}{L_T} + D_u \frac{R^2}{v_{th}} \frac{\partial \Omega_t}{\partial r} + RV_{pn} \tag{3.3}$$

where the terms on the right hand side represent, in order, the diffusion term, the thermo-diffusion term, due to the presence of a temperature gradient [11, 12], the roto-diffusion term [13, 14], due to the presence of a toroidal angular velocity gradient, and a pure convection term [15, 16] related to the curvature of the toroidal magnetic field. The coefficients D_T, D_u and term V_{pn} depend on the plasma micro-turbulence and so on the plasma gradients, therefore the equation (3.3) in general cannot be considered a linear relationship between the particle transport and the plasma gradients. In the case of trace impurities and in the radially local limit though, relation (3.3) becomes linear.

The experimental density peaking of the light impurities are compared to numerical simulations that calculate the neoclassical and the turbulent particle fluxes. For the calculation of the neoclassical contribution to the particle transport the code NEO [28, 29, 30] was used. For the turbulent fluxes, quasi-linear and non-linear gyro-kinetic simulations with the code GENE (Gyrokinetic Electromagnetic Numerical Experiment) [31, 32] have been done. GENE solves the gyro-kinetic Vlasov equations coupled with the Maxwell equations within a δf approximation [33] and using field aligned coordinates $\{x, y, z\}$, where z is the coordinate along the magnetic field line, x is the radial coordinate and y is the binormal coordinate. For a part of the quasi-linear study, also the code GKW (GyroKinetics at Warwick) [34, 35] in the local limit has been used. In particular, the GKW code was used in order to study the contribution of the roto-diffusion term as it allows to use different values of $\partial\Omega_t/\partial r$ for the different kinetic species considered in the simulation.

In stationary conditions, with no sources in the plasma core, equation (3.1) requires that $\Gamma_n = 0$. The density peaking is then calculated, using equation (3.2), as

$$\frac{R}{L_n}\left(\Gamma_n = 0\right) = -\frac{RV_n}{D_n}. \tag{3.4}$$

In the gyro-kinetic simulations, in order to evaluate the different terms in equation (3.3), N kinetic species of the light impurity under study (with charge Z, density n_Z, density gradient $R/L_{n,Z}$, temperature gradient

$R/L_{T,z}$ and rotation $\Omega_{t,Z}$) are used, that satisfy the conditions

$$\begin{aligned} n_Z^{exp} &= \textstyle\sum_{j=1}^{N} (n_Z)_j \\ \left(\frac{R}{L_{n,Z}}\right)_{exp} &= \frac{1}{N}\textstyle\sum_{j=1}^{N}\left(\frac{R}{L_{n,Z}}\right)_j \\ \left(\frac{R}{L_{T,Z}}\right)_{exp} &= \frac{1}{N}\textstyle\sum_{j=1}^{N}\left(\frac{R}{L_{T,Z}}\right)_j \\ \left(\frac{R^2}{v_{th}}\frac{\partial\Omega_{t,Z}}{\partial r}\right)_{exp} &= \frac{1}{N}\textstyle\sum_{j=1}^{N}\left(\frac{R^2}{v_{th}}\frac{\partial\Omega_{t,Z}}{\partial r}\right)_j . \end{aligned} \tag{3.5}$$

Simulations with N kinetic species of the same impurity that satisfy the conditions (3.5) are equivalent to simulations with one kinetic species of that impurity with the total density and gradients due to the linearity of the Vlasov equations with respect to the species. Linear simulations confirmed that, in our case, the light impurities cannot be considered as traces, as they have a non-negligible influence on the micro-instability growth rate, and that the conditions (3.5) must be satisfied. In order to study the role of the different terms in (3.3), 4 species of the same impurity have been considered in some quasi-linear simulations. By imposing to be non-zero only one of the three gradients in (3.3) ($R/L_{n,Z}, R/L_{T,Z}, \partial\Omega_{t,Z}/\partial r$) in each of the three species equations and using all zero gradients for the fourth species equation (to calculate the convective part), it is possible to calculate the contribution to the impurity particle flux from each of the terms in equation (3.3). This calculation has been carried out for Nitrogen.

In the quasi-linear simulations, a mixing length rule was employed [36, 37]. The mixing length rule used is based on the assumption that the turbulent diffusivity scales as

$$D \propto \frac{(\Delta x)^2}{\Delta t} = \frac{\gamma}{\langle k_\perp^2 \rangle} \tag{3.6}$$

where γ is the linear growth rate of the main micro-instability and $\langle k_\perp^2 \rangle$ can be written, taking into account the extended structure of the electrostatic potential ϕ along the field line, as

$$\langle k_\perp^2 \rangle = \frac{\int |\phi|^2 k_\perp^2 dxdz}{\int |\phi|^2 dxdz}.$$

$k_\perp$ is defined as $k_\perp^2 = k_y^2 g^{yy} + 2k_y k_x g^{xy} + k_x^2 g^{xx}$, where g^{ij} is the (i,j) component of the metric tensor g. The quasi-linear particle flux is then calculated as

$$\Gamma^{QL} = G \cdot \sum_{k_y} \Gamma_{k_y}^{norm} \frac{\gamma_{k_y}}{\langle k_\perp^2 \rangle} \tag{3.7}$$

where the linear particle transport for each value of k_y is normalized as $\Gamma_{k_y}^{norm} = \Gamma_{k_y}/\langle|\phi|^2\rangle$ and where G is a normalization factor. G, needed to reproduced the saturated non-linear fluxes, is left equal one in this case as it disappears in the calculation of $R/L_{n,Z}$ (equation 3.8). In all the quasi-linear simulations the range $0.1 \leq k_y\rho_s \leq 0.9$ is used, as higher k_y modes do not contribute to particle transport. In order to have reliable results, the condition $q_e^{QL}/q_i^{QL} \approx q_e^{exp}/q_i^{exp}$ was required (q^{QL} is calculated in a similar way as Γ^{QL}). The expected density peaking of the impurity under study is then calculated, using (3.7) with two species of the same impurity to calculate RV_n^{QL} (imposing $R/L_{n,Z} = 0$ for one of the two species) and D_n^{QL} and neglecting the neoclassical contribution (found negligible compared to the turbulent one), as

$$\frac{R}{L_{n,Z}} = -\frac{RV_n^{QL}}{D_n^{QL}}. \tag{3.8}$$

Tests were made in the quasi-linear simulations, changing $s, q, R/L_n, R/L_{Ti}, \Omega_t$ within the experimental error

#	ρ_{tor}	s	q	R/L_{ne}	R/L_{Te}	R/L_{Ti}	β_e	ν_{eff}	T_i/T_e
86740	0.33	0.4	1.2	2.8	7.9	4.5	0.2%	0.08	1.1
	0.5	0.8	1.9	2.8	7.8	5	0.1%	0.16	1.13
	0.7	1.4	2.6	3.5	13	8.5	0.06%	0.46	1.6
86749	0.33	0.4	1.2	2.8	8	4.7	0.25%	0.1	1.2
	0.5	1.1	1.6	2.9	7.9	6	0.14%	0.2	0.9
	0.7	1.5	2.5	3.9	16.5	10	0.06%	0.74	1.6
86758	0.33	0.4	1.2	2.2	6	8.5	0.5%	0.1	1.4
	0.5	1	1.5	2	7	5	0.3%	0.2	1.3
	0.7	1.6	2.5	3.8	10	7	0.1%	0.46	1.7
90670	0.33	0.4	1.6	3.3	8	5	0.33%	0.08	0.74
	0.5	0.8	1.9	2.4	8.2	4.5	0.17%	0.16	0.9
	0.7	1.3	2.8	3.3	13	9	0.08%	0.48	1.2

Table 1: Main plasma parameters of the studied discharges at the studied radii. $\nu_{eff} = 0.1 \cdot Z_{eff} n_e / T_e^2$ and $\beta_e = 4.03 \cdot 10^{-03} \cdot n_e T_e / B_0^2$ (n_e in 10^{19} units and T_e in keV).

range. The obtained variation of $R/L_{n,Z}$ is indicated by the error bars of the simulated values in table 2 and figure 3.

In the quasilinear gyro-kinetic simulations Miller geometry [39] was used as well as collisions, external flow shear and finite-β effects and the range $0.1 \leq k_y \rho_s \leq 1.2$ was used in the simulations. In the non-linear simulations the same settings were used and typical grid parameters were as follows: perpendicular box sizes $[L_x, L_y] \approx [190, 125]\rho_s$, phase-space grid discretization $[n_x, n_y, n_z, n_{v\parallel}, n_\mu] = [128-256, 24-64, 32, 32-64, 12-16]$, with $0.25 - 0.5 \leq k_y \rho_s \leq 1.6$, depending on the plasma radius, parameters and on the number of kinetic species considered. In all the simulations main ions and electrons are retained as kinetic species as well as the light impurity species under study. All the quasi-linear and non-linear gyro-kinetic simulations results shown in this work are from simulations carried out with the GENE code, except for the study of the role played by the roto-diffusion term in equation (3.3), that has been studied using the GKW code for the reasons explained above. Using the same input parameters, GENE and GKW quasi-linear simulations gave similar predictions for the light impurity density peaking in the studied cases. In this study we always consider fully ionized impurities.

4 Light impurity transport

The radial density profiles, measured with charge exchange, of the light impurities studied in this work are shown in *figure 2.* ^3He, Be and Ne profiles are peaked in the whole plasma core region while the profiles of N and C present a flat region inside $0.3 \lesssim \rho_{tor} \lesssim 0.7$. No substantial differences in the peaking of profiles of $^3He, Be$ and N have been observed between L-modes and in H-modes, indicating that the higher rotation, the higher fast D content or the higher plasma β in the H-modes are not modifying substantially the light impurity particle transport in the considered range of parameters (see *table 1*). Furthermore, similar $^3He, Be$ and Ne density profiles have been observed in discharges n. 90666, 90668, 90671 and 90672. In these shots 1.7 MW of NBI has been used, but the (on-axis, in ^3He minority scheme) ICRH power has been changed from 2.5 to 7 MW between the shots. This indicates that the amount of the on-axis ICRH ion heating is not affecting the light impurity transport in these discharges.

The input parameters in the numerical simulations (see *table 1*) have been taken from discharges:

- n. 86740, averaging on $9.5\,s < t < 10.5\,s$, for the study of C transport;
- n. 86749, averaging on $8\,s < t < 10\,s$, for the study of ^3He and N transport;
- n. 86758, averaging on $7.5\,s < t < 8.5\,s$, for the study of ^3He and N transport in H-modes;
- n. 90670, averaging on $5.8\,s < t < 6.4\,s$, for the study of $^3He, Be$ and Ne.

	Shot number	Radial position	Experimental	GENE QL	GENE NL
^3He	90670	$\rho_{tor} = 0.33$	3.5 ± 1.2	2.1 ± 0.3	-
		$\rho_{tor} = 0.5$	2.5 ± 1	1.0 ± 0.2	-
		$\rho_{tor} = 0.7$	4 ± 1.5	1.7 ± 0.2	-
Be	90670	$\rho_{tor} = 0.33$	2.5 ± 1.5	1.6 ± 0.1	-
		$\rho_{tor} = 0.5$	1.8 ± 1	1.4 ± 0.1	-
		$\rho_{tor} = 0.7$	4 ± 1.5	1.5 ± 0.1	-
C	86740	$\rho_{tor} = 0.33$	1 ± 1	1.5 ± 0.1	1.2 ± 0.2
		$\rho_{tor} = 0.5$	0 ± 1	1.5 ± 0.2	1 ± 0.2
		$\rho_{tor} = 0.7$	0 ± 1	1.6 ± 0.2	-
N	86749	$\rho_{tor} = 0.33$	1.8 ± 1.2	1.4 ± 0.2	2 ± 0.4
		$\rho_{tor} = 0.5$	0 ± 0.5	1.5 ± 0.3	1 ± 0.2
		$\rho_{tor} = 0.7$	4 ± 2	1.5 ± 0.2	-
Ne	90670	$\rho_{tor} = 0.33$	4 ± 2	1.7 ± 0.1	-
		$\rho_{tor} = 0.5$	1.8 ± 0.5	1.9 ± 0.1	-
		$\rho_{tor} = 0.7$	3 ± 1	1.7 ± 0.1	-

Table 2: *Experimental and predicted values (from quasi-linear and, for some cases, non-linear gyro-kinetic simulations) of the density peaking of the different light impurities in the plasma.*

Using the parameters of discharges n. 86740, 86749 and 86758 at $\rho_{tor} = 0.2, 0.33, 0.4, 0.5, 0.6, 0.7$, the contribution of the neoclassical transport to the particle transport of C and N was investigated with the NEO code. The neoclassical transport has been found to be negligible in the studied region, being $RV^{neo}/RV^{turb}, D^{neo}/D^{turb} \sim 10^{-2}$. To study the turbulent particle transport, gyro-kinetic quasi-linear and some non-linear simulations have been made, as discussed in section 3, at $\rho_{tor} = 0.33, 0.5, 0.7$. In the quasi-linear simulations the parameters were adjusted within error bars in order to match the experimental q_e/q_i while in the nonlinear simulations the experimental values of q_e and q_i have been reproduced within error bars. In the quasi-linear simulations, multiple light impurity species have been considered in some cases in order to study the possible impact of the presence of other light impurities on the peaking of the impurity under study. The impact of including multiple species has been found minimal. In the non-linear simulations, just one light impurity kinetic species per time has been considered. The results obtained from gyro-kinetic simulations are shown in *figure 3* and reported in *table 2*. The gyro-kinetic simulations always predict peaked density profiles for all the light impurities studied and no substantial differences in the peaking of the different impurities. In particular, the simulations never predict flat or hollow density profiles for C, N, in contrast to the experimental observations. The GKW simulations, made using 4 species for N at $\rho_{tor} = 0.5$ in order to study the role of the various terms in equation (3.3), predict a weak role of the roto-diffusion term. They predict that the thermo-diffusion term is $\sim 1/2$ of the geometrical convective term and the roto-diffusion term is $\sim 1/20$ of the geometrical convective term. They also predict the geometrical pinch term to be directed inward while the thermo-diffusion and the roto-diffusion terms to be directed outward. The negligible role of roto-diffusion, supported by comparisons between GENE simulations with and without the effects of the plasma toroidal rotation, is in agreement with the experimental observation that no differences in the light impurity radial profiles have been observed when introducing higher toroidal rotation using high NBI power. As for the other two terms, we cannot discriminate whether it is an overestimate of curvature pinch or an underestimate of the thermo-diffusion pinch (or possibly another mechanism) that leads to peaked simulated profiles instead of the flat experimental ones, because we do not have an independent experimental determination of the two terms, nor of the total convective and diffusive terms separately, which would require the employment of transient techniques of pulse propagation. With regard to the peaked impurity cases, some under-prediction of the impurity density peaking of the more peaked profiles has been observed.

In the above analysis we considered source free light impurity transport; this has been verified for all the impurities except for Ne at $\rho_{tor} \approx 0.7$, where a possible source has been found depending on the plasma parameters. Taking into account the source could modify the obtained results for Ne at this radial position but

does not change the overall picture. Also, the effects of the background neoclassical distribution function on turbulent particle transport have not been considered. These effects can affect in particular the roto-diffusion term [40], especially in presence of high plasma rotation. Nevertheless, in our case, due to the low plasma rotation in our discharges, they are not expected to change significantly the picture described above.

5 Discussion and conclusions

Radial density profiles of five light impurities, with $2 \leq Z \leq 10$, have been measured by active charge-exchange diagnostics in L-mode shots at JET with ITER-like wall, in conditions where turbulent transport is the dominant transport mechanism in the region of interest. Within the same discharge or very similar discharges, the profiles show different shapes, depending on the impurity Z. The ^3He, Be and Ne density profiles are peaked over the whole plasma core region, while C and N show a flat/hollow profile in the region $0.3 \lesssim \rho_{tor} \lesssim 0.7$. These observations add new experimental information to what observed in the past in JET L-mode and H-mode C-Wall plasmas [3, 5, 8]. Considering the various results on turbulent transport of light impurities published from JET and other devices together with the results in this paper, it seems there is a trend to observe peaked profiles for $Z = 2, 4$ impurities ($^3He, Be$), peaked or flat/hollow profiles, depending on the radial position and on the plasma parameters, for $Z = 5, 6, 7, 9$ impurities (B, C, N, F), and again peaked profiles for $Z = 10, 18$ impurities (Ne, Ar).

Neoclassical, quasi-linear and non-linear gyro-kinetic simulations have been carried out to explain the observed impurity density peaking. Our simulations predict similar peaking of the density profiles for all the light impurities studied and peaked profiles at all the studied radii. They tend to slightly underestimate the peaking of the more peaked profiles and never predict flat/hollow profiles. Quasi-linear gyro-kinetic simulations predict no big role of roto-diffusion, with respect to the geometrical pinch and to the thermo-diffusion, in the off-diagonal convective terms in equation 3.3. Whilst in previous modeling of high NBI power, highly rotating, JET H-modes [3, 5] roto-diffusion helped to reproduce the C hollow profiles, in our low NBI power cases the effects linked to rotation are small. Although recent studies indicate that when considering the effects of the background neoclassical distribution function, the roto-diffusion term can become more important [40], this is not expected to help in our case due to the low plasma rotation in our discharges (see figure 1). Therefore the origin of the mismatch between theoretical predictions and experimental results for these low rotation cases is still not understood and hopefully the work described in this paper will trigger further ideas in order to reproduce the experimental observations.

Acknowledgements

The authors would like to thank Yann Camenen, Athina Kappatou and Marco Valisa for precious suggestions and discussions. The authors are grateful to D. R. Mikkelsen for assistance. This research used resources of the National Energy Research Scientific Computing Center, a DOE Office of Science User Facility supported by the Office of Science of the U.S. Department of Energy under Contract No.DE--AC02--05CH11231. A part of this work was carried out using the HELIOS supercomputer system at Computational Simulation Centre of International Fusion Energy Research Centre (IFERC-CSC), Aomori, Japan, under the Broader Approach collaboration between Euratom and Japan, implemented by Fusion for Energy and JAEA. We acknowledge the CINECA award under the ISCRA initiative, for the availability of high performance computing resources and support. This work has been carried out within the framework of the EUROfusion Consortium and has received funding from the Euratom research and training programme 2014–2018 under grant agreement No 633053. The views and opinions expressed herein do not necessarily reflect those of the European Commission.

References

[1] Mandrekas J., Stacey W. M., Nucl. Fusion 35, 843 (1995).

[2] Pacher G. W., et al., Nucl. Fusion 47, 469 (2007).

[3] Manas P., et al., 16$^{\text{th}}$ ITPA Transport and Confinement Topical Group Meeting (ITPA T&C Meeting), Ahmedabad, India (2016).

[4] Angioni C., et al., Plasma Phys. Control. Fusion 51, 124017 (2009).

[5] Manas P. et al, Physics of Plasmas 24, 062511 (2017).

[6] Fable E., Angioni C. and Sauter O., Plasma Phys. Control. Fusion 52, 015007 (2010).

[7] Howard N. T., et al., Nucl. Fusion 52, 063002 (2012).

[8] Nordman H., et al., Plasma Phys. Control. Fusion 53, 105005 (2011)

[9] M. R. Wade et al., Journal of Nuclear Materials 290-293, 773 (2001).

[10] R. Dux et al., Plasma Phys. Control. Fusion 45, 1815 (2003).

[11] Coppi B. and Spight C., Phys. Rev. Lett. 41, 551 (1978).

[12] Weiland J., Jarm´en A.B. and Nordman H., Nucl. Fusion 29, 1810 (1989).

[13] Camenen Y., et al., Phys. Plasmas 16, 012503 (2009).

[14] Casson F. J., et al., Phys. Plasmas 17, 102305 (2010).

[15] Yankov V. V. , JETP Lett. 60, 171 (1994).

[16] Garbet X., et al., Phys. Rev. Lett. 91, 035001 (2003).

[17] Grierson B. A., et al., Phys. Plasmas 22, 055901 (2015).

[18] Van Eester D., et al., Plasma Phys. Control. Fusion 51, 044007 (2009).

[19] J. Hedin, et al., Nuclear Fusion 42, 527 (2002).

[20] T. Hellsten, et al., Nuclear Fusion 44, 892 (2004).

[21] C. Giroud et al., Rev. Sci. Instrum. 79, 10F525 (2008).

[22] M. G. von Hellermann et al., Phys. Scr. 2005 19, (2005).

[23] Fonck R. J., Darrow D. S. and Jaehnig K. P., Phys. Rev. A 29, 3288 (1984).

[24] Kappatou A., Ph.D. thesis: 'Investigations of helium transport in ASDEX Upgrade plasmas with charge exchange recombination spectroscopy', Eindhoven University of Technology Library, ISBN: 978-90-386-3704-4, NUR: 926 (2014).

[25] Hinton F. L. and Hazeltine R. D., Rev. Mod. Phys. 48, 239 (1976).

[26] Angioni C., et al., Nucl. Fusion 52, 114003 (2012).

[27] Angioni C. and Peeters A. G., Phys. Rev. Lett. 96, 095003 (2006).

[28] Belli E. A. and Candy J., Plasma Phys. Control. Fusion 50, 095010 (2008).

[29] Belli E. A. and Candy J., Plasma Phys. Control. Fusion 51, 075018 (2009).

[30] Belli E. A. and Candy J., Plasma Phys. Control. Fusion 54, 015015 (2012).

[31] Jenko F., et al., Phys. Plasmas 7, 1904 (2000).

[32] Görler T., et al., J. Comput. Phys. 230, 7053 (2011).

[33] Brizard A. J., Hahm T. S., Rev. Mod. Phys. 79, 421 (2007).

[34] A.G. Peeters, et al., Computer Physics Communications 180, 2650 (2009).

[35] A.G. Peeters, C. Angioni, D. Strintzi, Phys. Rev. Lett. 98, 265003 (2007).

[36] Jenko F., Dannert T. and Angioni C., Plasma Phys. Control. Fusion 47B, 195 (2005).

[37] Casati A., et al., Nucl. Fusion 49, 085012 (2009).

[38] Angioni C., Nucl. Fusion 51, 023006 (2011).

[39] Miller R. L., et al., Phys. Plasmas 5, 973 (1998).

[40] Manas P., et al., Plasma Phys. Control. Fusion 59, 035002 (2017).

Figures

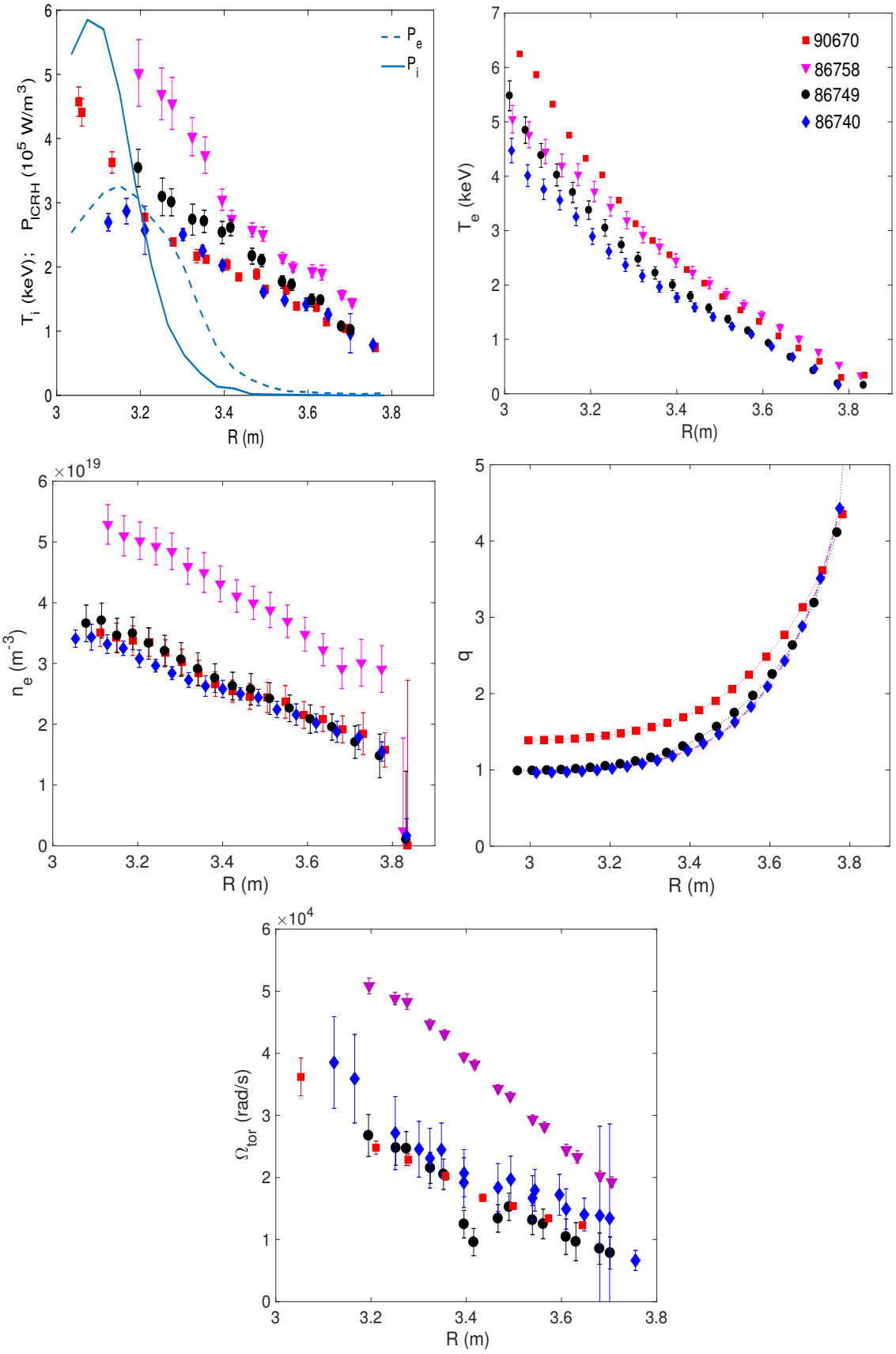

Figure 1: *Radial profiles of T_i, T_e, n_e, q and Ω_t of JET discharges n. 86740 at $t = 10$ s (blue pentagons), n. 86749 at $t = 9$ s (black circles), n. 86758 at $t = 8$ s (magenta triangles) and n. 90670 at $t = 6$ s (red squares). The ICRH power deposition, obtained with the SELFO code, is also shown for discharge n. 90670.*

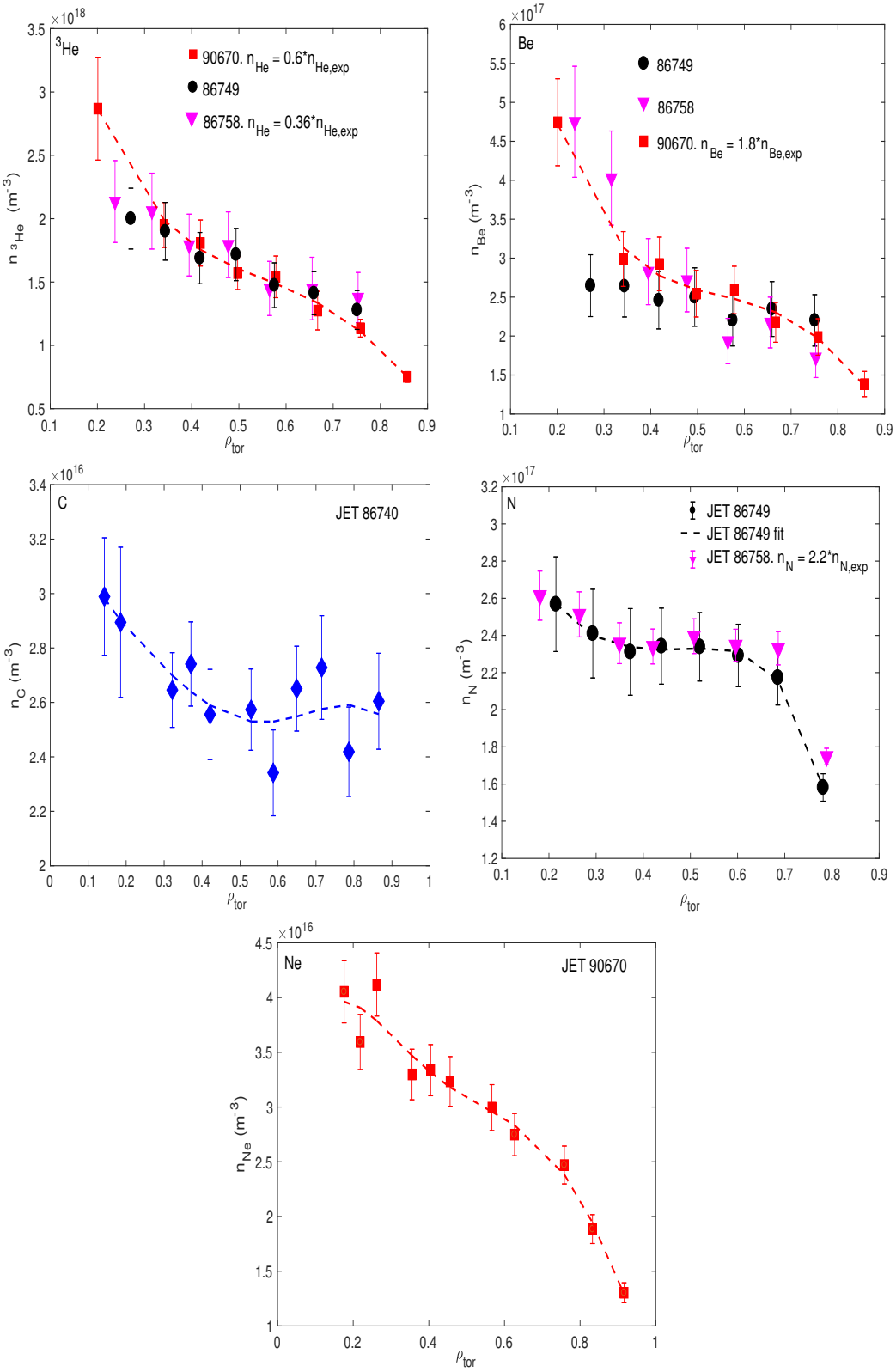

Figure 2: *Radial density profiles of ^3He, Be, C, N, and Ne. The profiles are taken from JET discharges n. 86740 (3 MW of ICRH + 4 MW of NBI) at t = 10s (blue diamonds), n. 86749 (4 MW of ICRH + 4 MW of NBI) at t = 9s (black circles), n. 86758 (4 MW of ICRH + 13 MW of NBI) at t = 8 s (magenta triangles) and n. 90670 (6 MW of ICRH + 1.7 MW of NBI) at t = 6.2s (red squares). Some of the profiles are rescaled, as indicated, for a better comparison between different discharges.*

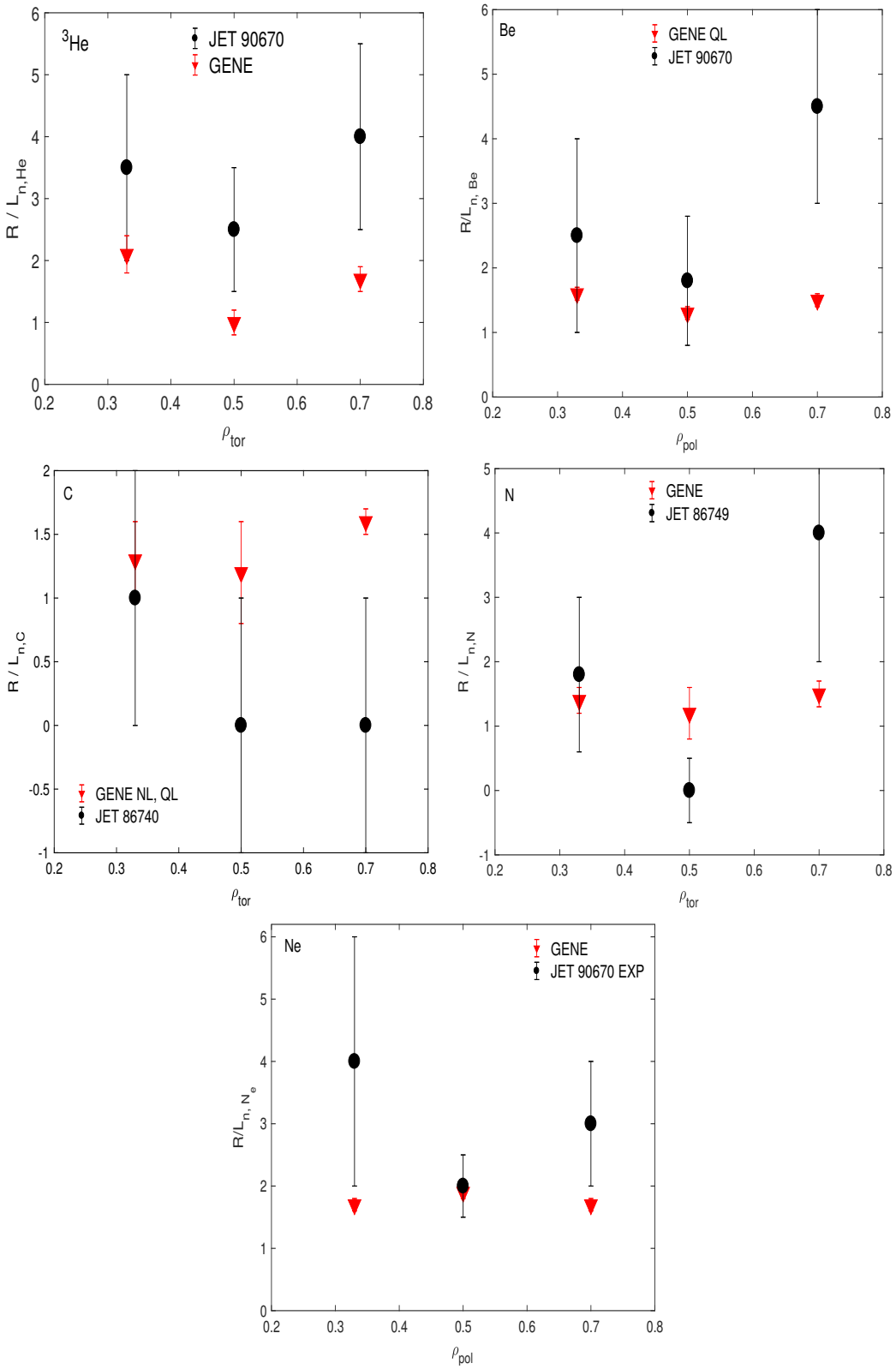

Figure 3: *Normalized density peaking at* $\rho_{tor} = 0.33, 0.5, 0.7$ *of* ^3He*, Be, C, N, and Ne for JET discharges n. 86740 (3 MW of ICRH + 4 MW of NBI) at t = 10s, n. 86749 (4 MW of ICRH + 4 MW of NBI) at t = 9s and n. 90670 (6 MW of ICRH + 1.7 MW of NBI) at t = 6.2s. The experimental values are indicated with black circles. The best results from the gyro-kinetic simulations (quasi-linear and non-linear) are indicated by red triangles.*